Characterization of Concentration- and Use-dependent Effects of Quinidine from Conduction Delay and Declining Conduction Velocity in Canine Purkinje Fibers

Douglas L. Packer, Augustus O. Grant, Harold C. Strauss, and C. Frank Starmer
Division of Cardiology, Department of Medicine, and the Departments of Computer Science and Pharmacology, Duke University Medical Center, Durham, North Carolina 27710

Abstract

The dynamic response of squared conduction velocity, θ^2, to repetitive stimulation in canine Purkinje fibers with quinidine was studied using a double-microelectrode technique. With stimulation, a frequency-dependent monoexponential increase in conduction delay (CD) and a decline in θ^2 were observed. The exponential rates and changes in steady-state CD and θ^2 were frequency- and concentration-dependent. The overall drug uptake rates describing blockade and the interpulse recovery interval were linearly related and steady-state values of θ^2 were linearly related to an exponential function of the stimulus intervals. Based on first-order binding, the frequency- and concentration-dependent properties of quinidine were characterized by the apparent binding and unbinding rates of 14.2±5.7 $\times 10^6$ $mol^{-1} \cdot s^{-1}$ and 63±12 s^{-1} for activated and 14.8±1.0 $\times 10^2$ $mol^{-1} \cdot s^{-1}$ and 0.16±0.03 s^{-1} for resting states. The recovery time constant extracted from the pulse train interpulse interval was 5.8±1.5 s compared with 5.1±0.6 s determined from a posttrain test pulse protocol. This study demonstrates that the kinetics of drug action can be derived from measures of impulse propagation. This provides a basis for characterizing frequency-dependent properties of antiarrhythmic agents in vivo and suggests the plausibility of a quantitative assessment of drug binding and recovery rates in man.

Introduction

The fundamental role of the inward sodium current (I_{Na})[1] as the driving force behind impulse propagation is indicated by the conduction modification accompanying alterations in sodium channel conductance. Declining conduction velocity (θ) or other measures of conduction delay (CD) have been shown to accompany both the decline in $\dot{V}_{max}$ produced by a reduction in extracellular sodium concentration (1) and drug-induced sodium channel blockade (2–12). Despite such qualitative observations, the precise mathematical relationship between measures of channel conductance and impulse propagation has been more difficult to specify.

Investigations to explore this relationship have nevertheless been made on both theoretical and experimental levels. Donati and Kunav (13) in studying θ in unmyelinated axons have shown that in the absence of contaminating currents, the squared conduction velocity, θ^2, is directly proportional to the product of available sodium channel conductance and a function dependent on the threshold of excitability. Walton and Fozzard (14) demonstrated experimentally a nearly linear relationship between peak inward ionic current normalized by the capacitance that is filled during the upstroke of the action potential and θ. The cable equation adapted for the physiologic setting by Hodgkin and Rushton (15) also predicts a theoretical linear relationship between early net membrane currents and θ^2. In a study showing quinidine and procainamide-induced use-dependent modification of θ^2 in guinea pig papillary muscle, Buchanan and co-workers (11) provided experimental verification of a 1:1 relationship between steady-state $\dot{V}_{max}$ and θ^2 over a wide range of drug concentrations and stimulus frequencies. Nevertheless, kinetic studies fully characterizing the relationship between these parameters under transient or dynamic conditions have not been available.

Antiarrhythmic drug modification of I_{Na} has been extensively characterized. Johnson and McKinnon (16) demonstrated that the degree of quinidine-induced depression of $\dot{V}_{max}$ in guinea pig ventricular muscle was a function of the stimulation frequency. This observation has subsequently been confirmed in both nerve and cardiac tissue (17–22), and has led to the term use dependence (19) to describe the accumulation of channel blockade occurring with repetitive stimulation. Although other studies have demonstrated analogous use-dependent CD in animals (6, 7, 11, 23) and in humans (8–10, 24), complete parallel kinetic studies from measures of conduction have not been available.

We have previously shown that the drug-induced reduction of peak I_{Na}, which follows an exponential time course, allows estimation of apparent binding and unbinding rates (25). Assuming a near linear relationship between sodium conductance and θ^2, it follows that in the presence of drug, small transient changes in θ^2 occurring over a pulse train should likewise follow an exponential time course. This pattern of blockade accumulation should also allow the determination of apparent binding and unbinding rate constants from measures of propagation. Because description of the kinetic and steady-state effects of antiarrhythmic agents in humans remains dependent on demonstrable changes in CD, this capability could be useful in understanding further the mechanism of action and quantifying the effects of antiarrhythmic agents in man.

Address reprint requests to Dr. Douglas L. Packer, Mayo Foundation, Rochester, MN 55905.

Received for publication 25 July 1988 and in revised form 21 February 1989.

1. *Abbreviations used in this paper:* APD, action potential duration at 90% repolarization; CD, conduction delay; I_{Na}, inward sodium current; ISI, interstimulus intervals; τ_r, time constant of recovery from blockade; θ, conduction velocity; θ^2, squared conduction velocity; V_m, membrane potential.

J. Clin. Invest.

0021-9738/89/06/2109/11 $2.00
Volume 83, June 1989, 2109–2119

With this focus on clarifying the dynamic modification of impulse propagation by antiarrhythmic agents and its relationship to channel activity, we sought to (*a*) develop a kinetic description of the onset of and recovery from use-dependent channel blockade manifest by declining θ^2 and CD as measures of conduction in a simple propagating system; and (*b*) determine whether the kinetics of blockade recovery can be extracted from the recovery interval between two consecutive pulses of a drive train.

We found that the frequency and concentration-dependent properties of quinidine can be characterized by a set of frequency-independent rate constants derived from CD and θ^2, suggesting that under appropriate conditions, measures of conduction might be used to more completely characterize drug effects in humans. Preliminary reports of this study have recently appeared in abstract form (26, 27).

Methods

Experiments were performed on unbranched Purkinje fibers obtained from 15–25-kg mongrel dogs after 30 mg/kg pentobarbital anesthesia i.v. Fiber dissection was completed in high potassium cardioplegia solution after rapid excision of the heart. Fibers > 1 cm long were fixed in a lucite chamber and superfused for 1 h with control Tyrode's solution containing (in millimolar: 120, NaCl; 22, HCO_3; 5, dextrose; 0.5, $MgCl_2$; 0.5, NaH_2PO_4; 2.5, $CaCl_2$; and 5.4, KCl. Temperature was maintained at 36.5±0.5°C using a constant temperature circulator and pH at 7.40±0.05 by equilibration with a gas mixture of 95% O_2 and 5% CO_2. The superfusate flow rate was maintained at 8–10 ml/min.

The transmembrane potential (V_m) was recorded from two microelectrodes positioned in the middle and distal end of the Purkinje fiber. The interelectrode distance, determined using a calibrated eyepiece, ranged between 3.8 and 9.2 mm (mean = 5.5±1.5 mm). Microelectrodes beveled to a resistance of 8–16 mΩ were filled with 3 M KCl and coupled via a Ag/AgCl wire to a high impedance microprobe system (WPI 700; World Precision Instruments, New Haven, CT). V_m and a 100-ms time marker were simultaneously displayed on an oscilloscope (model 565; Tektronix, Inc., Beaverton, OR) and photographed on 35-mm film using a kymographic camera (Model C4; Grass Instruments, Quincy, MA). Action potential duration (APD-90) and V_m were measured directly from the film. The signal from each microelectrode was also differentiated electronically using an analogue differentiator and sample-hold peak detection circuit, modified from Hondeghem and Cotner (28). The derivative was filtered and held for 90 ms to allow recording on a strip chart recorder (model 2200, Gould Inc., Cleveland, OH) at a paper speed of 5 mm/s (Fig. 1). The recording system was linear over a range from 200–1,000 V/s. An interval timing circuit was used to determine the interelectrode conduction time from the peak $\dot{V}_{max}$ at each microelectrode. The $\dot{V}_{max}$ from the proximal and distal microelectrodes and the conduction time were digitized from the strip chart records for subsequent data analysis. θ^2 was determined from the interelectrode distance and corresponding conduction time. Although $\dot{V}_{max}$ may be an imperfect reflection of sodium conductance, the application of the microelectrode technique facilitated the study of conduction and the comparison of use-dependent drug blockade manifest by incremental CD, θ^2, and $\dot{V}_{max}$ under physiologic temperatures, which would have been impossible under voltage clamp.

Stimulation protocol. The Purkinje fiber was stimulated near its end using a pair of silver wires positioned at a distance of 4–6 mm proximal to the first electrode, using 1.0 ms constant current pulses at a strength of 1.5–3 times diastolic threshold. Drug uptake, as indicated by incremental CD and θ^2, was assessed using 20-s pulse trains with interstimulus intervals (ISIs) within the train of 1.5, 1.0, 0.9, 0.8, 0.7, 0.6, 0.5, and 0.4 s. 20 s was allowed between each pulse train to permit complete recovery from blockade. After control observations, the fibers were superfused with 4 μg/ml quinidine gluconate (7.6×10^{-6} M) or 8 μg/ml (1.52×10^{-5} M) with at least 1 h allowed for equilibration. Quinidine was used due to its relatively long recovery time constant with respect to channel gate reactivation. Quinidine is an open-state blocking agent with little plateau phase blockade (29–31), as also indicated by the absence of impact of APD on overall blockade (32). Only those experiments in which a single impalement was maintained throughout both control and quinidine studies are reported. Continuous longitudinal conduction via a single pathway during the pulse train was presumed if a single continuous curve relating incremental CD and pulse number was present. Fibers showing discontinuous conduction during drug uptake or recovery were discarded. Recovery from blockade during that interval was sampled with a test pulse introduced from 0.5 to 20 s after pulse trains with 0.50 or 0.75 s ISIs (Fig. 1). The time constants of recovery (τ_r) were derived from the reciprocal slope of the regression of the natural log of residual phasic blockade against recovery time. Uptake and recovery studies were repeated to test reproducibility.

Analytical methods. We assumed that θ^2 was related to the available sodium conductance in terms of an unknown function of sodium conductance, $f(g_{Na})$, such that

$$\theta^2 = f(g_{Na}) \quad (1)$$

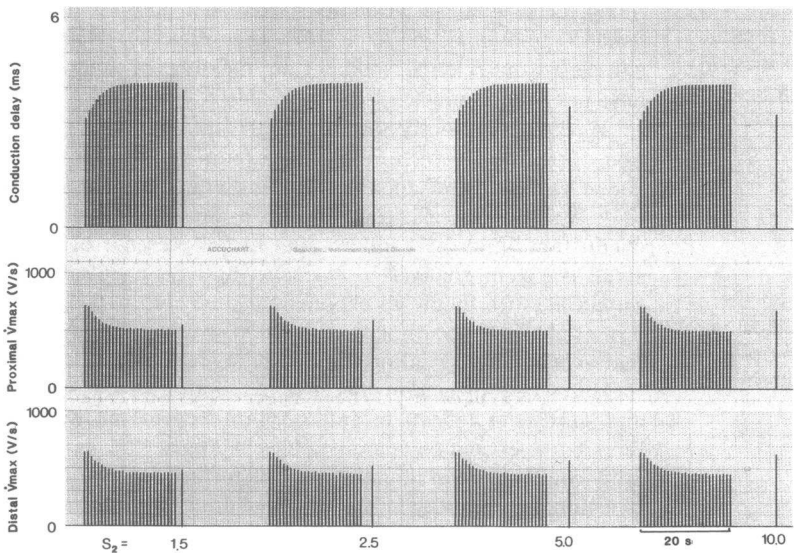

Figure 1. Actual analogue data demonstrating the time course of use-dependent drug-channel interaction. The top channel shows the stepwise incremental CD observed over a 20-s pulse train with a 0.75-s interpulse interval. The middle and lower channels similarly demonstrate the stepwise decline in $\dot{V}_{max}$ simultaneously recorded from the proximal and distal microelectrodes, respectively. Also shown is the sampling of recovery 0.75–20 s into the interpulse recovery interval after accumulation of blockade during the pulse train. With successively longer recovery periods, the incremental CD and $\dot{V}_{max}$ depression acquired during the pulse train return toward their respective control values.

and for small changes in g_{Na}, the function f can be approximated by a linear relationship of the form:

$$\theta^2 = f(\bar{g}_{Na}) + df/dg_{Na}(g_{Na} - \bar{g}_{Na}) \quad (2)$$

We further assume that channel blockade reduces the available sodium conductance according to

$$g_{Na} = \bar{g}_{Na}(1 - b_n) \quad (3)$$

where b_n is the fraction of blocked channels associated with the nth stimulus. Assuming that repetitive stimulation cycles the channels between mixtures of activated and resting binding states, block associated with the nth pulse is described by the relationship

$$b_n = b_{ss} + (b_0 - b_{ss})e^{-n\lambda^*} \quad (4)$$

where b_0 is the initial and b_{ss} is the steady-state blockade, and b_n is the blockade associated with the nth pulse.

The time course of channel blockade was determined from the use-dependent incremental prolongation of conduction time as well as from declining θ^2 using a nonlinear least squares exponential fitting procedure. This yielded an apparent drug uptake rate constant, λ^*, and a steady-state blockade value (b_{ss}) from CD and θ^2 with each pulse train of constant ISI. Parallel analyses were performed for use-dependent declining $\dot{V}_{max}$ from the proximal and distal microelectrodes and from θ. In several fibers spontaneous diastolic depolarization during the recovery interval contributed to a decrease in the first pulse $\dot{V}_{max}$ of the next pulse train. In these fibers, the first pulse was omitted from the analysis to facilitate exponential fitting.

The quantitative methodology of the guarded receptor approach as previously described (25, 33–39) and derived in detail in the Appendix, was used to estimate the drug uptake rates for the activated (λ_a) and the resting states (λ_r) as well as activated (a_∞) and resting (r_∞) equilibrium blockade. From these apparent binding and unbinding rate constants, k_a and l_a for activated and k_r and l_r for resting states were estimated from CD and θ^2. In so doing, a two-state (activated and resting) model of blockade was adopted and negligible binding and unbinding during the inactivation interval was assumed. This is consistent with the previous observations of several investigators who found quinidine blockade to occur predominately during open-channel access with little evidence of block of inactivated channels (29–31).

The predicted or expected time course of θ^2 reduction was simulated using these derived rate constants in the expression: θ^2 = maximal $\theta^2(1 - b_n)$, where b_n is related to λ^* as shown in Eq. 4. A family of expected values for a variety of stimulus rates not used in the derivation of the binding affinities were then obtained by varying only the ISI.

In determining the steady-state relationship between θ^2 and the corresponding $\dot{V}_{max}$ measured at the proximal electrode in the presence of drug, the observed values of both measures at each interstimulus interval were normalized to the respective control values at the longest paced interstimulus interval under control conditions. Similarly in assessing the dynamic relationship between θ^2 and $\dot{V}_{max}$ in the presence of drug, the normalized declining θ^2 occurring over each pulse of a single train was compared with the normalized companion $\dot{V}_{max}$.

The significance of differences between time constants and binding rates based on conduction measurements and $\dot{V}_{max}$ was determined using a paired t test or one-way analysis of variance where appropriate. All data are reported as the mean±SD.

Results

Action potential characteristics. V_m during pulse train stimulation under control conditions measured −85.9±5.2 mV (range −79.0 to −94.9 mV) immediately upon return of the action potential to baseline. In the presence of quinidine, the V_m upon repolarization measured −86.7±5.8 mV (range −78.5 to −95.5 mV). The take-off potential under control conditions measured −83.2±5.8 mV (range −75.3–92.0 mV) at the end of 20-s pause between pulse trains and underwent no significant change to the −82.4±6.1 mV value (range −75.2–91.0 mV) observed with quinidine. An actual increase in the negativity of V_m at the take-off point was seen in three fibers, whereas a 0.3–2.4-mV depolarization was noted in five fibers. One additional fiber showed a 3.2-mV depolarization. No indication of any significant concentration-dependent effect of quinidine on V_m was observed.

The APD-90 in the control state averaged 345±39 ms (range 320 to 420 ms). In the presence of quinidine, the APD-90 declined to 307±22 ms (range 280 to 340 ms) (P = 0.02). No difference in action potential characteristics was observed between fibers superfused with 4 vs. 8 μg/ml of quinidine.

Quinidine-induced conduction delay. The conduction time over the 5.5±1.5 mm (range 3.8 to 9.2 mm) interelectrode distance under control conditions measured 2.99±0.87 ms (range 1.48 to 4.66 ms), with < 5% variation at each ISI and no consistent decline in conduction time over the pulse train. Assuming one-dimensional impulse propagation in the Purkinje fiber; θ for each ISI averaged 1.89±0.52 M/s (range 1.42 to 3.38 M/s) yielding a θ^2 of 3.66±2.65 M^2/s^2 in the control state.

Significant use-dependent channel blockade was manifest by incremental CD occurring over the course of the pulse train as shown in Fig. 2 for ISIs of 1.5, 0.8, and 0.5 s. A corresponding decline in θ^2 over the pulse train was likewise observed. The respective prolongation of CD as well as decline in θ and θ^2 proceeded until steady state was achieved, with the greatest steady-state blockade observed at the shortest ISI. Steady-state values for each indicator of drug-channel interaction with 4 or 8 μg/ml quinidine at ISIs of 1.0 and 0.5 s are shown in Table I. Conduction time prolonged 33% at the longer and 55% at the shorter ISI. θ declined 24 and 35%, respectively, at the same ISIs, whereas the change in θ^2 (37 and 54%, respectively) paralleled that observed with CD and $\dot{V}_{max}$. With 8 μg/ml quinidine, a greater prolongation of conduction time was observed with a 41% increase over control at the 1.0-s ISI and 65% increase at the 0.5-s ISI, 10% greater than observed at the 4 μg/ml concentration. θ^2 likewise underwent a 50% decline at the longer and 63% decline at the 0.5-s ISI.

The time course of use-dependent CD or declining θ^2 could be adequately fit by an exponential expression, yielding an overall drug uptake rate, λ^*, for each ISI as also shown in Fig. 2. The greatest apparent drug uptake per pulse was observed with the slowest pacing rates. The λ^*'s derived from each of the three measures of conduction modification by quinidine were equivalent.

The predicted linear relationship between λ^* derived from CD and θ^2 and the accompanying interpulse recovery interval (t_r = ISI − APD) was linear as shown for θ^2 in Fig. 3. A similar linear relationship was observed when λ^* was derived from $\dot{V}_{max}$. The activated state uptake rate constant, λ_a, at 4 μg/ml derived from the y-intercept of this relationship averaged 112±5 s^{-1} using information derived from CD and was 149±12 s^{-1} from θ^2. In fibers superfused with 8 μg/ml quinidine, λ_a was significantly larger than those at the lower concentration, as shown in Table II: 187±35 s^{-1} from CD (P < 0.001), and 252±54 s^{-1} from θ^2 (P < 0.005). The time constants of acquisition of blockade, τ_a, where $\tau_a = 1/\lambda_a = (k_aD + l_a)^{-1}$ was therefore greater at the lower drug concentration of 4 μg/ml than at 8 μg/ml (Table II).

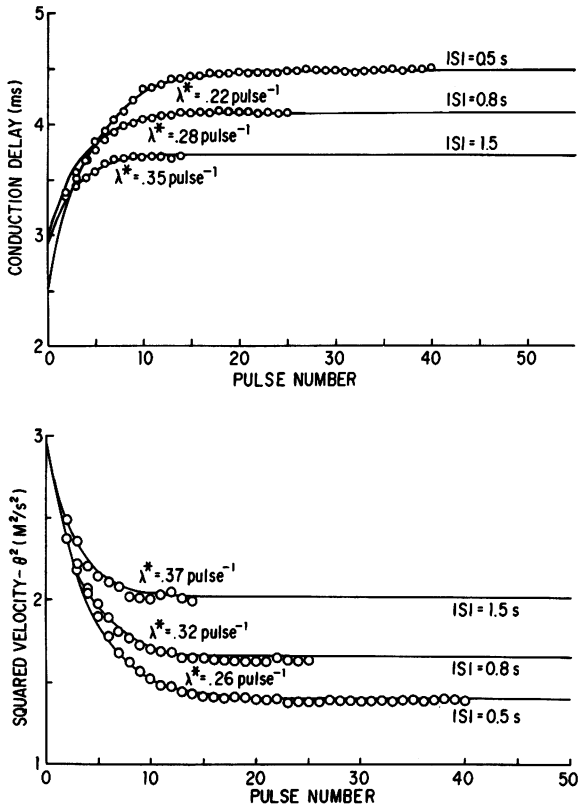

Figure 2. Use-dependent channel blockade manifest by incremental CD and declining θ^2 in the presence of 8 μg/ml quinidine. (*Top*) The stepwise increase in CD occurring with each pulse of a 20-s train at ISIs of 1.5, 0.8, and 0.5 s. The accumulation of delay continues until steady state is reached, with greater steady-state blockade observed at shorter ISIs. (*Bottom*) The corresponding declining θ^2 occurring with each pulse. A nonlinear, least squares technique was used to fit an exponential equation to each set of experimental data, allowing derivation of the descriptive drug uptake rate constant, λ^*, (pulse^{-1}) for each ISI.

The resting-state drug uptake rate constant, λ_r, was determined from 11 fibers using the slope of the relationship between λ^* and τ_r, as also shown in Fig. 3. λ_r derived from CD was 0.15±0.03 s^{-1} and 0.16±0.04 s^{-1} from θ^2 with 4 μg/ml quinidine and 0.19±0.05 s^{-1} and 0.21±0.03 s^{-1} at 8 μg/ml quinidine, respectively. The difference between λ_r derived from these sources was not significant. In contrast to observed differences in λ_a, λ_r was independent of quinidine concentration. Equivalent drug uptake rates were derived from use-dependent changes in V_{max} (Table III).

Table I. Steady-State Conduction Modification with 4 or 8 μg/ml Quinidine

		4 μg/ml (five fibers)		8 μg/ml (six fibers)	
	ISI	Control	Quinidine	Control	Quinidine
CD (*ms*)	1.0	3.49±0.96	4.31±0.96	2.59±0.72	3.61±1.08
	0.5		4.93±1.07		4.23±1.10
θ (*M/s*)	1.0	1.79±0.18	1.44±0.12	1.98±0.71	1.46±0.41
	0.5		1.27±0.13		1.19±0.36
θ^2 (M^2/s^2)	1.0	3.24±0.66	2.11±0.36	4.34±3.52	2.28±1.40
	0.5		1.62±0.34		1.53±1.03
$\dot{V}_{max}$ (*prox*)	1.0	783±113	538±68	750±113	407±92
(*V/s*)	0.5		425±54		315±94

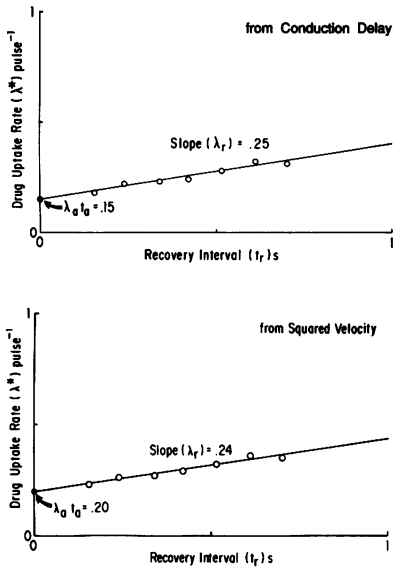

Figure 3. Linear regression of the overall drug uptake rate, λ^*, against the interstimulus or recovery interval, t_r. (*Top*) Plot of λ^* obtained from CD on the y axis against t_r on the x axis, yields a *y*-intercept of $\lambda_a t_a$, from which the activated- or excited-state uptake rate, λ_a, is derived. t_a is the mean channel open time. The slope of this relationship yields the resting state uptake rate, λ_r. Here $\lambda_a = k_a D + l_a$ and $\lambda_r = k_r D + l_r$. (*Bottom*) Equivalent information derived from θ^2.

Activated and resting equilibrium blockade. The steady-state term, γ, as derived in Eq. 10 (see Appendix) was estimated for each preparation using λ^* and λ_r. The activated or excited state equilibrium blockade, a_∞, was determined from the *y*-intercept of the regression of steady-state blockade for each ISI with the corresponding γ, as shown in Fig. 4. As seen, the relationship is linear as predicted. Comparable results were obtained from CD and $\dot{V}_{max}$. The values for the activated state equilibrium blockade derived from CD and θ^2 in the presence of 4 and 8 μg/ml quinidine are given in Table II. Significantly higher fractional equilibrium blockade with 8 μg/ml was noted in each of the measure of impulse propagation. In addition, a_∞ obtained from θ^2 was almost two times greater than that observed than derived from θ.

The resting equilibrium blockade or tonic blockade, r_∞, could also be quantified from the slope of the relationship shown in Fig. 4 without the bias created by drug uptake occurring during a traditional test pulse. As seen in Table III, a trend towards greater r_∞ in the presence of 8 μg/ml of quinidine compared with 4 μg/ml was seen, although the difference was not significant. The activated and resting-state binding equilibria, determined from changes in $\dot{V}_{max}$ recorded at the proximal microelectrode, are also shown for comparison in Tables II and III.

Observed relationship between θ^2 and $\dot{V}_{max}$. The microelectrode technique also permitted an assessment of the relationship between drug-induced changes in measures of propagation and local net membrane sodium current, to the extent it is reflected by $\dot{V}_{max}$ at physiologic temperatures. In all fibers, the relationship between steady-state θ^2 and $\dot{V}_{max}$ (normalized to control values at 2.0 s ISI) was linear, with an average correlation coefficient of 0.98±0.02. The average slope in seven fibers was 1.02±0.13 (range 0.91 to 1.24) without forcing the relationship through (0, 0) or (1, 1). The slope of the relationship was > 1 and < 1 in two fibers each. The change in steady-state θ^2 tracked the accompanying decline in $\dot{V}_{max}$ better than did the change in θ.

Table II. Concentration-dependent Activated-State Uptake Rates (λ_a), Uptake Time Constants (τ_a), and Equilibrium Blockade (a_∞) with 4 and 8 μg/ml Quinidine

	λ_a (s^{-1})		τ_a (ms)		a_∞	
			μg/ml			
	4	8	4	8	4	8
CD (*ms*)	112±5	187±35*	9.0±0.3	5.5±1.1*	0.59±0.10	0.82±0.11‡
θ (*M/s*)	135±10	228±45*	7.4±0.6	4.7±1.0*	0.38±0.04	0.46±0.03*
θ^2 (M^2/s^2)	149±12	252±54*	6.7±0.6	4.1±0.8*	0.63±0.05	0.72±0.04‡
$\dot{V}_{max}$ (*prox*) (*V/s*)	126±27	236±42*	8.2±1.8	4.4±7.0*	0.63±0.06	0.68±0.07
			* $P < 0.005$	‡ $P < 0.05$		

P values describe significance levels of differences in λ_a or τ_a between 4 and 8 μg/ml quinidine.

This relationship between θ^2 and $\dot{V}_{max}$ was also evident under the transient conditions of pulse train stimulation. With repetitive stimulation at 0.4 s, the pulse by pulse declining normalized $\dot{V}_{max}$ and accompanying θ^2 were linearly related, with a mean slope of 1.1±0.3 (range 0.97–1.25) as shown superimposed from eight fibers in Fig. 5. No consistent departure from this relationship was noted at an ISI of 0.4 s compared with 0.8 or 1.5 s, as might have been expected with any significant change in passive membrane properties during the pulse train.

Apparent rate constants. The calculated forward and reverse apparent drug binding rate constants are shown in Table IV. Because the estimates of forward and reverse rate constants were independent of drug concentration, the results given in Table IV reflect the pooled values for both 4 and 8 μg/ml concentrations. In the activated state, the forward binding constant k_a derived from CD averaged 11.5±5.5 × 10^6 $M^{-1} \cdot s^{-1}$ (range 6.4 to 13.9 × 10^6 $mol^{-1} \cdot s^{-1}$). Using θ^2 as a measure of use-dependent drug-channel interaction yielded a k_a of 14.2±5.7 × 10^6 $mol^{-1} \cdot s^{-1}$ (range 8.5 to 16.0 × 10^6 $mol^{-1} \cdot s^{-1}$). Values derived from declining θ and $\dot{V}_{max}$ are also given in Table IV. The resting-state uptake rate constant k_r (also given in $mol^{-1} \cdot s^{-1}$) was, in general, four orders of magnitude smaller than that observed in the accessible state, with an average value of 0.77±1.7 × 10^2 from incremental CD and 14.8±1.0 × 10^2 from θ^2, respectively. When expressed in terms of k_aD and k_rD in the presence of 1.52 × 10^{-5} M quinidine, ~ 150 binding events occur per second at activated potentials with only 0.02 s^{-1} occurring at a resting V_m, supporting prior studies in which k_r was presumed to be 0 (29, 30, 40).

The reverse rate constant, l_a, for unbinding in the activated state at excited potentials, is also given in Table IV. l_a was 38±17 s^{-1} (range 7 to 57 s^{-1}) as derived from CD, and 63±12 s^{-1} (range 44 to 81 s^{-1}) when derived from θ^2. The reverse or unbinding rate constants for recovered channels at resting potentials, l_r, was 0.18±0.04 s^{-1} (range 0.13 to 0.24 s^{-1}) using incremental CD, and was 0.16±0.03 (range 0.11 to 0.20) from θ^2. At activated potentials, l_a, was 200–500 times larger than l_r, suggesting greater unblocking from open channels during the activated interval or conversely that unbinding from resting channels is impeded. The forward and reverse apparent binding rate constants as derived from changes in proximal $\dot{V}_{max}$ were: k_a = 12.1±4.5 × 10^6 $mol^{-1} \cdot s^{-1}$; l_a = 63±25 s^{-1}, k_r = 15.3±15.1 × 102 $mol^{-1} \cdot s^{-1}$, and l_r = 0.18±0.03 s^{-1}, which were equivalent to those derived from θ^2 or CD.

Simulations of use-dependent channel blockade. These forward and reverse apparent rate constants at activated and resting potentials were then used to predict tonic and steady-state quinidine blockade, as well as λ^* for a series of stimulation rates. Varying only the ISI, a family of curves describing the predicted time course of use-dependent drug-channel interaction in terms of incremental CD and declining θ^2 was derived. Fig. 6 shows the observed and predicted prolongation in CD and decline in θ^2 in the presence of 8 μg/ml quinidine for ISIs of 1.5, 0.8, and 0.5 s.

Recovery from quinidine-induced blockade. The kinetics of recovery from quinidine blockade, determined using a test pulse to sample recovery 0.75–20 s after blockade produced by pulse train stimulation using ISIs of 0.75 or 0.5 s, could be characterized from CD and θ^2. τ_r derived from the slope of the

Table III. Resting-State Equilibrium Blockade (r_∞), Drug Uptake Rate (λ_r), and Time Constants of Recovery (τ_r) from Quinidine Blockade

	r_∞		λ_r				
			μg/ml				
	4	8	4	8	τ_{r750}	τ_{r500}	τ_{rup}
CD (*ms*)	0.01±0.01	0.01±0.01	0.15±0.03	0.19±0.05	4.2±1.0	4.1±0.5	6.2±1.3*‡
θ (*M/s*)	0.03±0.04	0.03±0.03	0.16±0.03	0.20±0.05	4.8±1.0	4.9±0.5	6.0±1.4
θ^2 (M^2/s^2)	0.07±0.07	0.11±0.06	0.16±0.04	0.21±0.03	5.0±1.3	5.1±0.6	5.8±1.5
$\dot{V}_{max}$ (*prox*) (*V/s*)	0.06±0.05	0.12±0.13	0.20±0.03	0.18±0.04	4.3±1.4	4.8±1.4	5.3±0.8

*‡ Significance of difference at $P < 0.05$ level between τ_{rup} and τ_{750} and τ_{rup} and τ_{r500}, respectively when derived from CD; τ_{r750} = time constant of recovery from blockade generated by 20-s pulse train with 750 ms interstimulus intervals; τ_{r500} = recovery time constant after 20-s pulse train with 500 ms interstimulus intervals; τ_{rup} = recovery time constant extracted from the interstimulus interval of the pulse train.

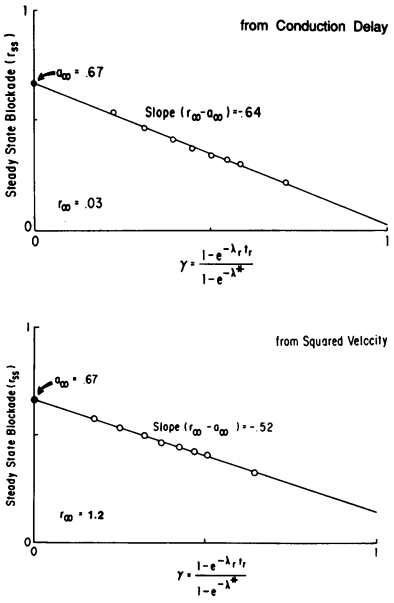

Figure 4. Relationship between steady-state blockade (r_{ss}) and the equilibrium expression $\gamma = (1 - e^{-\lambda_r t_r})/1 - e^{-\lambda^*}$ as derived from incremental CD (*top*) and θ^2 (*bottom*). The *y*-intercept yields the activated or excited state equilibrium value, a_∞. Resting or tonic blockade, r_∞, is derived from the slope of the regression, $r_\infty - a_\infty$. Here, $a_\infty = k_a D/k_a D + l_a$ and $r_\infty = k_r D + l_r$ giving the final two equations necessary to derive k_a, l_a, k_r, and l_r.

regression of the natural log of residual blockade expressed in terms of CD against τ_r using this traditional methods is shown in Fig. 7 *A*. Here, the recovery rate constant was 0.20 s^{-1}, yielding a τ_r of 5.0 s. Fig. 7 *B* shows τ_{rup} extracted from the recovery interval between successive pulses of an uptake drive train from conduction delay, represented as the slope of the relationship between λ^* and the ISI or recovery interval using methods displayed in Fig. 3. Here $\lambda_r = 0.18$ s^{-1}, yielding a τ_{rup} of 5.5 s. Reasonable agreement was also observed between τ_{rup} and τ_r describing recovery from blockade manifest as depressed $\dot{V}_{max}$.

The results from the recovery assessment in eight fibers are summarized in Table III. τ_r using the poststimulation method as well as the time constant of recovery extracted from the ISI of drug uptake pulse trains, τ_{rup}, were derived from use-dependent CD, θ^2, θ, and proximal $\dot{V}_{max}$ as markers of drug effect. τ_r determined after pulse train stimulation was independent of

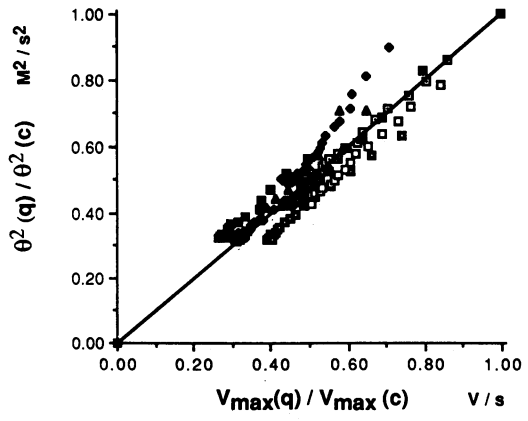

Figure 5. Dynamic relationship between normalized $\dot{V}_{max}$ and normalized θ^2 over the course of a pulse train in the presence of 4 or 8 μg/ml quinidine. The normalized θ^2 for each pulse of a 20-s pulse train with a 0.4-s interstimulus interval in eight fibers is plotted as a function of the normalized accompanying $\dot{V}_{max}$. The mean slope of the relationship was 1.1±0.3. Also shown is the unity line indicating a 1:1 proportional relationship.

Table IV. Directly Quantified Apparent Rate Constants

	k_a (× 10^6)	l_a	k_r (× 10^2)	l_r
	$mol^{-1} \cdot s^{-1}$	s^{-1}	$mol^{-1} s^{-1}$	s^{-1}
CD	11.5±5.5	38±17	0.77±1.7	0.18±0.04
θ	8.1±3.4	104±26	4.3±5.6	0.18±0.03
θ^2	14.2±5.7	63±12	14.8±1.0	0.16±0.03
$\dot{V}_{max}$ (*prox*)	12.1±4.5	63±25	15.3±15.1	0.18±0.03

both concentration and pulse train stimulation rate. Most importantly, we observed no significant difference between τ_{rup} extracted from the ISI of the pulse train and poststimulation τ_r, although a trend towards a slightly longer τ_{rup} was observed. This trend reached significance only when using incremental CD but not θ^2 as the indicator of use-dependent drug effect.

Discussion

In this study, we have demonstrated that quinidine induces a frequency-dependent decline in θ^2 and CD over a pulse train

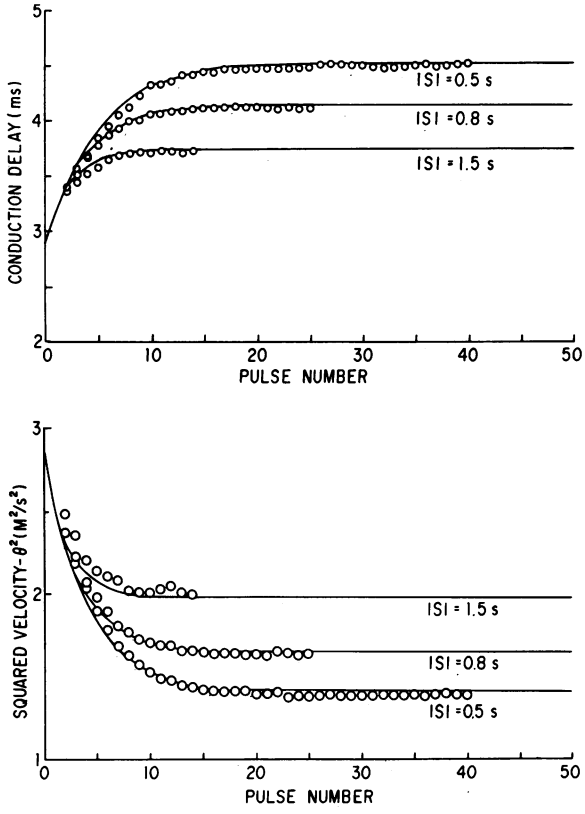

Figure 6. Observed and predicted accumulation of blockade in the presence of 8 μg/ml quinidine. The experimentally determined forward and reverse apparent rate constants for quinidine blockade were used to compute tonic and steady-state block and the interval-dependent uptake rate constant, λ^*. These values were then used to derive a predicted time course for use-dependent blockade in terms of incremental CD (*top*) and θ^2 (*bottom*). Varying only the interstimulus interval, predicted curves for intervals of 1.5, 0.8, and 0.5 s were generated (——). The agreement between these predictions and the actual experimental data points (o) was excellent for declining θ^2 and incremental CD. The predicted time course for CD was adjusted to accommodate tonic blockade.

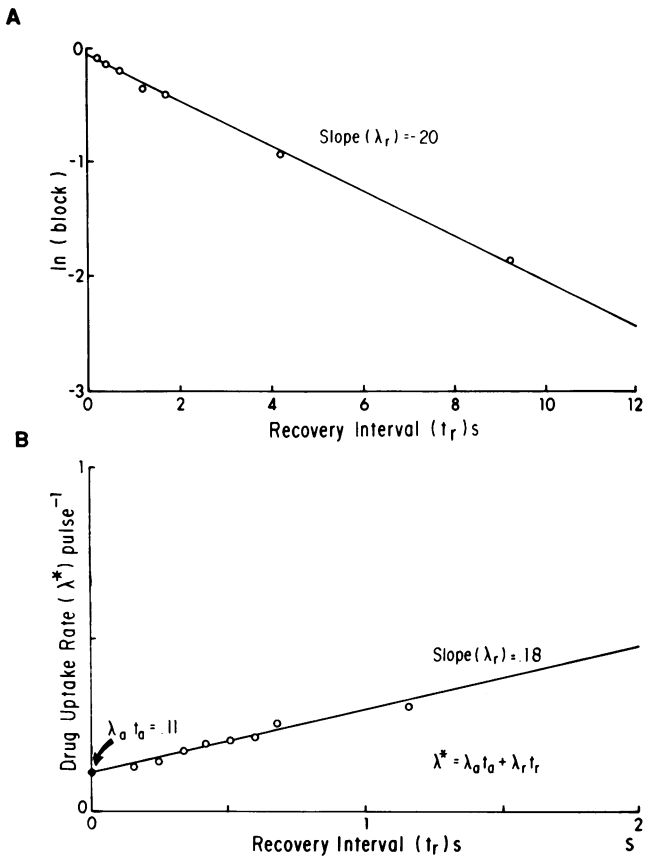

Figure 7. Recovery kinetics determined from use-dependent incremental CD. (*A*) The recovery rate constant derived using the post-stimulation method. Here the recovery rate constant, λ_r, is the slope of the relationship between the log of recovering phasic block and recovery time, t_r, measured 0.20 s^{-1}, giving a time constant, τ_r, of 5 s. (*B*) The recovery time constant, τ_{rup}, extracted from the interstimulus interval of a pulse train. The regression of the individual drug uptakes from CD and the respective ISIs was linear, yielding a slope or recovery rate constant of 0.18 s^{-1} or a τ_{rup} of 5.5 s, showing reasonable agreement between the two methods.

and that the magnitude of blockade was concentration dependent. This study goes beyond the demonstration of use-dependent conduction delay under steady-state conditions, however, and demonstrates that changes in incremental CD and θ^2 due to this antiarrhythmic agent follow an exponential time course, consistent with a simple first order model of drug-membrane interaction. Exploiting this property, apparent binding rate constants, that succinctly characterize the effects of quinidine in propagating systems independent of stimulation frequency and drug concentration, can be estimated. Furthermore, the kinetics of recovery from quinidine blockade can be extracted from the recovery interval between consecutive pulses of a drive train using incremental CD or θ^2 as the measure of blockade. Note also that under the conditions of this study, steady-state and dynamic changes in θ^2 tracked changes in $\dot{V}_{max}$, in the absence of any attempt to constrain propagation.

Conduction delay/use dependence. The accumulation of channel blockade manifest by declining I_{Na} or $\dot{V}_{max}$ occurring over a train of pulses, with greater steady-state blockade acquired at more rapid stimulation rates has been described for a variety of local anesthetics (16–22, 40–43). Other investigators have similarly shown use dependence on a tissue or intact organ level manifest by incremental conduction delay (6–10, 23, 24, 44). While these earlier in vivo observations are important, they reflect steady-state conditions without fully specifying the kinetics of the acquisition of and recovery from blockade. Additionally, study techniques in these investigations would not permit an assessment of the relationship between θ and channel blockade in the presence of drugs.

Subsequent inroads into this relationship have been recently made. Buchanan and co-workers (11) explored the relationship between θ^2 and $\dot{V}_{max}$ in guinea pig papillary muscle in the presence of varying concentrations of quinidine or procainamide. They demonstrated a 1:1 linear relationship between the normalized steady-state values of these parameters over a range of drug concentrations. We also noted this relationship and observed further that θ^2 and $\dot{V}_{max}$ were linearly related under the transient conditions prevailing during a single pulse train. Because of questions regarding the relationship between g_{Na} and $\dot{V}_{max}$ (45–50), however, the nature of the relationship between θ^2 and actual sodium current remains unclear. The findings of this study supports our assumption of a linear relationship between small changes in θ^2 and small changes in g_{Na}. This assumption is also consistent with recent theoretical work (13).

Further investigation of the kinetics of antiarrhythmic action, whether they be manifest by declining I_{Na} in vitro or incremental CD in vivo requires a simplified means of describing drug-channel interaction. In addition to steady-state information, these studies demonstrate that incremental CD and declining θ^2 in the presence of 4–8 μg/ml quinidine follow a monoexponential time course and show a linear relationship between the overall drug uptake rates and the interstimulus intervals. These findings are sufficient to allow the estimation of forward and reverse apparent rate constants (25, 34–39) and therefore permit a more detailed description of the frequency and concentration-dependent effects of quinidine. The apparent rate constants k_a and k_r derived from CD and θ^2 were found to closely track those obtained from declining $\dot{V}_{max}$, thus providing additional evidence for the relationship between θ^2 and measures of net early membrane current.

Characterization of the unbinding process. The estimated unbinding rate constants also provide insight into the kinetics of recovery from quinidine blockade. l_a ranged between 34 and 100 s^{-1}, in contrast to earlier estimates that were 5–10-fold higher (40). The l_r of $\sim$ 0.18 s^{-1} was in agreement with the findings of Weld et al. (29) who observed an l_r of 0.22 s^{-1} at equivalent potentials in ovine Purkinje fibers. Information derived from τ_r in Grant et al. (51) suggests further that l_r should be $\leq$ 0.25 s^{-1}, which is also in the range of our observations.

The 200–500-fold difference in l_a and l_r provides evidence that unbinding at resting potentials is constrained. Egression of the predominately charged quinidine moiety at physiologic pH from the channel interior would be expected to occur via the hydrophilic pathway at a rate proportional to the fraction of channels with an open or untrapped conformation (39, 43). During initial depolarization with stimulation, unbinding of drug-complexed channels is facilitated as reflected by the greater activated unbinding rate constant, l_a. In contrast, at resting potentials the fraction of untrapped drug-complexed channels is reduced, forcing recovery to proceed via the hydrophobic pathway after deprotonation. This additional step may explain the 4–6-s τ_r from quinidine blockade. Similar

trapping of the permanently charged QX compounds has been reported by other investigators (18, 25, 52, 53) who demonstrated accelerated recovery from blockade with membrane clamping to depolarized V_ms. Because quinidine with a pK_a of 8.6 is predominantly in the charged form at physiologic pH, trapping similar to that observed with the QX compounds should not be surprising. Because the rate of recovery from channel blockade is slowed with small subthreshold depolarizations (29, 41, 54–56) yet is markedly accelerated by depolarization as shown by I_a, the rate of recovery appears to pass through a critical minimal value at intermediate membrane V_m (25).

This study also demonstrates that the kinetics of recovery can be comparably described using CD and θ^2 as the measure of channel blockade. Excellent agreement was noted between those τ_rs derived from CD, θ^2, as well as $\dot{V}_{max}$. These findings complement those of Nattel (12), who in studies of canine Purkinje fibers exposed to 18–74 μM lidocaine also observed a monoexponential recovery process and agreement between recovery time constants derived from both recovering $\dot{V}_{max}$ and conduction delay. At higher concentrations (147 μM) general agreement between τ_rs derived from conduction delay and $\dot{V}_{max}$ was also observed, although the recovery process deviated from a perfectly linear relationship at the shortest recovery intervals. This suggested a nonexponential recovery phase when described by changes in conduction delay but not $\dot{V}_{max}$. We saw no consistent comparable deviation from a truly monoexponential recovery process from incremental conduction delay with either 4 or 8 μg/ml quinidine, however.

The time course of recovery from drug-channel blockade, extracted from drug uptake pulse train studies, was also found to be in reasonable experimental agreement with those determined applying traditional methods. In both cases the kinetics of recovery were independent of the initial level of blockade as previously shown (29, 30, 51). Both methods provided τ_rs of 4–6 s, which agree closely with the 4–10-s values previously reported (17, 29, 51).

The small difference in recovery rate constants may be related to slightly less negative membrane potentials at the take off point of the action potential producing expected prolongation of recovery time (29, 40, 41, 53, 56). This might be related to an accumulation of extracellular K^+ with pacing (55, 57–61) or the effect of incomplete recovery from the preceding action potential. Both effects might be expected to yield greater λ^*s, particularly at faster pacing rates, and thus flatten the slope of the relationship between λ^* and τ_r as shown in Fig. 3. Nevertheless, this difference is insignificant and the agreement between both methods provides strong support for the assumptions made in the model.

From k_r and I_r, equilibrium blockade at resting V_m or tonic blockade can also be predicted without the first pulse bias found using traditional techniques. Such bias might develop because of drug uptake in the test pulse or arise because of any increase in inactivated channels accompanying a small decline in resting V_m occurring during the prolonged diastolic interval. The guarded receptor approach, however, allows for tonic blockade determination from pulse train stimulation independent of these effects. The 3% tonic blockade observed in these conduction studies is consistent with earlier reports (22, 54), and also argues against any appreciable contribution of diastolic changes in resting V_m to total blockade.

Limitations of the study. The interpretation of these data may be limited by several factors inherent to the study methods used. To facilitate this evaluation of conduction, the microelectrode technique was required. This technique permitted the parallel analysis of θ^2 and sodium channel activity to the extent that it is reflected by $\dot{V}_{max}$ at physiologic temperatures. Good agreement between these measures of conduction and conductance under steady-state and dynamic conditions, as reflected in the apparent binding constants, was present. Nevertheless, the precise relationship between $\dot{V}_{max}$ and g_{Na} remains unclear, with several authors proposing (15, 45, 46) and others disputing (47, 48, 56) a linear relationship between these indicators of sodium channel availability. Recently, data provided by Fozzard et al. (49), although showing nonlinearity in the relationship between $\dot{V}_{max}$ and g_{Na} suggested that the overestimation of g_{Na} by $\dot{V}_{max}$ was small in the range of the $\dot{V}_{max}$ change and temperature present in this study. A subsequent study demonstrated, however, that quinidine may alter further the relationship of $\dot{V}_{max}$ to I_{Na} in single cardiac Purkinje cells (50). This study demonstrated that $\dot{V}_{max}$ overestimated I_{Na} at test potentials to −30 mV and underestimated at potentials to +30 mV. No data were available for test potentials in the −20 to +20-mV range as observed in this study. Because of this, the affinities determined from θ^2, although relating closely to $\dot{V}_{max}$ as a reflection of net early membrane current, may deviate from g_{Na}-derived values. Certainly apparent affinities derived under voltage-clamped conditions would be useful to validate these rate constants. This approach, however, would have prohibited the evaluation of conduction modification by quinidine. Given the theoretical relationship between θ^2 and conductance (13, 14), these affinities should still provide information useful in quantifying binding and comparing the effects of antiarrhythmic agents in a propagating system.

This study is also potentially limited by the inability to control the APD in this propagating system. This would be required to partition between activated- and inactivated-state blockade. In this case of the conducted action potential, however, assumptions regarding access time were required. Quinidine was therefore selected as the study agent, given its propensity for exclusive open-channel blockade (29–31). Previous work has also demonstrated little effect of pulse duration on total blockade (32). This absence of appreciable inactivation-state blockade thereby justifies the assumption that blockade occurs during the activation time, which is equivalent to the mean channel open time.

It is anticipated that this approach could be most easily extrapolated to describe blockade by other open channel blockers. Nevertheless, drug-channel interaction by more hydrophobic agents producing inactivated state blockade such as etidocaine and W36027 has been described using the total pulse duration as the accessible state duration (34, 37, 63). Rate constants describing blockade by both active and inactive state blockade can be also derived (63, 64) suggesting application of this model to describe blockade by a variety of pharmacologic agents.

Finally, because passive membrane properties were not assessed in this study, a possibility of confounding changes in R_i, R_m, or C_m known also to influence θ, cannot be excluded. A recent study by Arnsdorf and Sawicki (65) however, showed little change in these indices with the exception of R_m. The absence of consistent departure from the 1:1 relationship between θ^2 and $\dot{V}_{max}$ over the course of drive train at faster stimulation rates appears to militate against any significant changes

in passive membrane properties under the constraints of these study methods.

Implications. The ability to characterize antiarrhythmic drug action from CD has several important clinical and experimental implications. The ability to describe succinctly quinidine behavior with simple apparent forward and reverse binding rate constants from measures of conduction in vitro suggests that with appropriate extension and validation, the characterizing of action of antiarrhythmic drugs in man may be possible. The potential advantage of this information over that available in the plasma drug level for guiding therapy is appreciable. Furthermore, the demonstration that the kinetics of recovery can be extracted from the interval between two consecutive pulses of a pulse train also suggests a means of evaluating the time course of recovery from blockade induced by drugs with relatively long time constants in the clinical setting, in which prolonged poststimulation quiescent periods, required for traditional analysis of recovery, are impossible. This approach to drug uptake and recovery should facilitate future comparative studies of antiarrhythmic drug modification of propagation under normal or ischemic conditions and allow the assessment of the effect of single or combinations of antiarrhythmic agents, structure-activity relationships or proarrhythmic effects in vitro and in vivo.

Appendix

Additional analytical methods

The forward and reverse rate constants for quinidine binding were determined using the guarded receptor formalism (33–39).

With this approach, channels are viewed as voltage-dependent mixtures of accessible or inaccessible conformations. During stimulation or switching to activated potentials, the equilibrium shifts to favor a channel mixture in which accessible or unguarded channel conformations predominate, allowing drug access and binding to the receptor to occur. Upon return to resting potentials, the equilibrium shifts such that inaccessible or guarded channel conformations dominate the mixture.

This approach predicts that the time course of blockade during a train of pulses can be described by a piecewise exponential process. For a two-mixture process, this produces an alternating sequence of two exponentials, where the first describes drug uptake occurring at activated potentials when accessible channels predominate (34). The fraction of blocked channels at the end of accessible phase, a_0, can be written as:

$$a_0 = r_0 e^{-\lambda_a t_a} + a_\infty (1 - e^{-\lambda_a t_a}) \tag{1}$$

where r_0 is the amount of blockade before that activation and the exponential expression $e^{-\lambda_a t_a}$ describes drug uptake between those two points. Here t_a is equal to the interval of time the binding site is accessible and λ_a equals the activated drug uptake rate constant $1/\tau_a = k_a D + l_a$.

Similarly, the second exponential describes drug recovery occurring during the interstimulus interval between two pulses of a train. Here,

$$r_1 = a_0 e^{-\lambda_r t_r} + r_\infty (1 - e^{-\lambda_r t_r}) \tag{2}$$

where r_1 reflects the amount of blockade after the recovery interval and a_0 is the fraction of blocked channels prior to recovery, along with the exponential $e^{-\lambda_r t_r}$ describing the time course of recovery between those two points. t_r is the recovery time between pulses, and λ_r is the recovery rate constant or $1/\tau_r = k_r D + l_r$. An additional prediction of the model is that recovery occurring between two pulses of a train and that occurring after cessation of the drive train stimulation are equivalent in terms of time course. A description of the kinetics of recovering should therefore be available from this interstimulus recovery interval.

Blockade associated with the nth pulse of a train can be described recursively in terms of blockade acquired during the preceding pulse by the relationship:

$$a_{n+1} = a_n e^{-(\lambda_a t_a + \lambda_r t_r)} + r_\infty (1 - e^{-\lambda_r t_r}) e^{-\lambda_a t_a} + a_\infty (1 - e^{-\lambda_a t_a}) \tag{3}$$

This defines the overall drug uptake rate, λ^*, as the weighted sum of the two state-dependent uptake rates

$$\lambda^* = \lambda_a t_a + \lambda_r t_r \tag{4}$$

which predicts a linear relationship between λ^*, determined from an exponential fit to declining $\dot{V}_{max}$ or incremental conduction delay at any given interstimulus interval and t_r, the recovery interval between pulses. For open-channel blockade as expected with quinidine (29, 31–32), t_a is presumed to be the mean channel open time, which is assumed to be constant during pulse train stimulation (66). We have used a value of 1 ms for the mean channel open time, which is consistent with experimental studies (67). This assumption is only valid for exclusive open-channel blocking agents. In the case of plateau- or inactivated-state blockers, the pulse duration would be used as t_a. The slope of the relationship is λ_r, where

$$\lambda_r = \frac{1}{\tau_r} = k_r D + l_r \tag{5}$$

where k_r is the forward rate constant and l_r is the reverse rate constant for binding occurring at resting potentials. The intercept $\lambda_a t_a$ yields the activated state uptake rate, where

$$\lambda_a = \frac{1}{\tau_a} = k_a D + l_a \tag{6}$$

Here k_a is the forward and l_a is the reverse activated state rate constant.

With repetitive stimulation, steady-state is reached, which can be described in terms of the recursive relationship for the fraction of block immediately before depolarization:

$$r_{ss} = \frac{a_\infty (1 - e^{-\lambda_a t_a}) e^{-\lambda_r t_r} + r_\infty (1 - e^{-\lambda_r t_r})}{1 - e^{-\lambda^*}} \tag{7}$$

where a_∞ is the activated state and r_∞ is the resting state equilibrium. The fraction of block immediately after depolarization at steady state can be comparably derived. Here a_∞ and r_∞ are respectively given by:

$$a_\infty = \frac{k_a D}{k_a D + l_a} \tag{8}$$

$$r_\infty = \frac{k_r D}{k_r D + l_r} \tag{9}$$

Eq. 7 can be rewritten in terms of the constant γ and $1 - \gamma$, where

$$\gamma = \frac{1 - e^{-\lambda_r t_r}}{1 - e^{-\lambda^*}} \tag{10}$$

$$1 - \gamma = \frac{(1 - e^{-\lambda_a t_a}) e^{-\lambda_r t_r}}{1 - e^{-\lambda^*}} \tag{11}$$

giving the simplified expression

$$r_{ss} = a_\infty + \gamma (r_\infty - a_\infty) \tag{12}$$

This equation gives the final fundamental prediction of the guarded receptor approach: that steady-state blockade, r_{ss}, is a linear function of the state-dependent equilibria, a_∞ and r_∞. A plot of the regression of r_{ss} against γ allows determination of a_∞ from the intercept and r_∞ from the slope. The simultaneous solution of Eqs. 5, 6, 8, and 9 permit the estimation of the state-dependent binding rate constants, k_a, l_a, k_r, and l_r. Using appropriate guarding and trapping functions, the gating effects can be factored from the state-dependent rate constants to permit determination of the true forward and reverse rate constants, k and l.

Acknowledgments

We wish to acknowledge the kind assistance of Yvonne Walker, Jo Smaltz, and Re Dellia Powell in the preparation of this manuscript, and the technical expertise of Nick Jensen in the development of the instrumentation.

This work was supported in part by grants HL-17670, HL-19216, HL-32708, and HL-32994 from the National Institutes of Health, and the Walker P. Inman Memorial Fund, Duke University Medical Center.

References

1. Walton, M. K., and H. A. Fozzard. 1983. Experimental study of the conducted action potential in cardiac Purkinje strands. *Biophys. J.* 44:1–8.

2. Weidmann, S. 1955. Effects of calcium ions and local anesthetics on electrical properties of Purkinje fibers. *J. Physiol. (Lond.).* 129:568–582.

3. Gettes, L. S., B. Surawicz, and J. C. Shiue. 1962. Effect of high K, low K, and quinidine on QRS duration and ventricular action potential. *Am. J. Physiol.* 203:1135–1140.

4. Nattel, S. 1987. The relationship between frequency-dependence of local anesthetic drug effects on $\dot{V}_{max}$ and conduction in canine cardiac Purkinje fibers. *J. Pharmacol. Exp. Ther.* 241:282.

5. Nattel, S., V. Elharrar, D. P. Zipes, and J. C. Bailey. 1981. pH-dependent electrophysiological effects of quinidine and lidocaine on canine cardiac Purkinje fibers. *Circ. Res.* 48:55–61.

6. Davis, J., T. Matsubara, M. M. Scheinman, B. Katzung, and L. H. Hondeghem. 1986. Use-dependent effects of lidocaine on conduction in canine myocardium: application of the modulated receptor hypothesis in vivo. *Circulation.* 74:205–214.

7. Nattel, S. 1985. Frequency-dependent effects of amitriptyline on ventricular conduction and cardiac rhythm in dogs. *Circulation.* 72:898–906.

8. Morady, F., L. DiCarlo, J. Boerman, and B. Crevey. 1985. Rate-dependent effects of intravenous lidocaine, procainamide and amiodarone on intraventricular conduction. *J. Am. Coll. Cardiol.* 6:179–185.

9. Mercer, A. B., J. R. Foster, R. J. Simpson, and L. S. Gettes. 1983. Use-dependency of antiarrhythmic drugs in the human heart. *Circulation.* 68(Suppl. III):296. (Abstr.)

10. Gang, E. S., T. A. Denton, D. S. Oseran, W. J. Mandel, and T. Peter. 1985. Rate-dependent effects of procainamide on His-Purkinje conduction in man. *Am. J. Cardiol.* 55:1525–1529.

11. Buchanan, J. W., T. Sarto, and L. S. Gettes. 1985. The effects of antiarrhythmic drugs, stimulation frequency, and potassium-induced resting membrane potential changes on conduction velocity and dV/dt_{max} in guinea pig myocardium. *Circ. Res.* 56:696–703.

12. Nattel, S. 1987. Interval-dependent effects of lidocaine on conduction in canine cardiac Purkinje fibers: experimental observations and theoretical analysis. *J. Pharmacol. Exp. Ther.* 241:275–281.

13. Donati, F., and H. Kunov. 1976. A model for studying velocity variations in unmyelinated axons. IEEE (*Inst. Electr. Electron. Eng.*) Trans. on Biomed. Eng. 23:23–28.

14. Walton, M. K., and H. A. Fozzard. 1983. The conducted action potential: models and comparison to experiments. *Biophys. J.* 44:9–26.

15. Hodgkin, A. L., and W. A. H. Rushton. 1946. The electrical constants of a crustacean nerve fiber. *Proc. R. Soc. Lond.* B. *Biol. Sci.* 133:444–479.

16. Johnson, E. A., and M. G. McKinnon. 1957. The differential effect of quinidine and pyrilamine on the myocardial action potential at various rates of stimulation. *J. Pharmacol. Exp. Ther.* 120:460–468.

17. Heistracher, P. 1971. Mechanism of action of antifibrillatory drugs. *Naunyn-Schmiedeberg's Arch. Pharmakol.* 269:199–212.

18. Strichartz, G. R. 1973. The inhibition of sodium current in myelinated nerve by quaternary derivatives of lidocaine. *J. Gen. Physiol.* 62:37–57.

19. Courtney, K. R. 1975. Mechanism of frequency-dependent inhibition of sodium currents in frog myelinated nerve by the lidocaine derivative GEA 968. *J. Pharmacol. Exp. Ther.* 195:225–236.

20. Schwarz, W., P. T. Palade, and B. Hille. 1977. Local anesthetics: effect of pH on use-dependent block of sodium channels in frog muscle. *Biophys. J.* 20:343–368.

21. Kohlhardt, M., and C. Seifert. 1980. Inhibition of $\dot{V}_{max}$ of the action potential by propafenone and its voltage, time, and pH dependence in mammalian ventricular myocardium. *Naunyn-Schmiedeberg's Arch. Pharmacol.* 315:55–62.

22. Colatsky, T. J. 1982. Quinidine block of cardiac sodium channels is rate- and voltage-dependent. *Biophys. J.* 37:343*a*. (Abstr.)

23. Talajic, M., and S. Nattel. 1986. Frequency-dependent effects of calcium antagonist on atrioventricular conduction and refractoriness: demonstration and characterization in anesthetized dogs. *Circulation.* 74:1156–1167.

24. Ellenbogen, K. A., L. D. German, W. G. O'Callaghan, P. G. Colavita, A. C. Marchese, M. R. Gilbert, and H. C. Strauss. 1985. Frequency-dependent effects of verapamil on atrioventricular nodal conduction in man. *Circulation.* 72:344–352.

25. Starmer, C. F., J. Z. Yeh, and J. Tanguy. 1986. A quantitative description of QX222 blockade of sodium channels in squid axons. *Biophys. J.* 49:913–920.

26. Packer, D. L., A. O. Grant, H. C. Strauss, and C. F. Starmer. 1986. Determination of apparent binding affinities from use-dependent conduction delay and $\dot{V}_{max}$ reduction in Purkinje fibers. *Circulation.* 74:253. (Abstr.)

27. Packer, D. L., A. O. Grant, H. C. Strauss, and C. F. Starmer. 1986. Quantitative determination of recovery kinetics from use-dependent drug uptake: a test of the guarded receptor hypothesis. *Circulation.* 74:20. (Abstr.)

28. Hondeghem, L. M., and C. K. Cotner. 1978. Measurement of $\dot{V}_{max}$ of the cardiac action potential with a sample/hold peak detector. *Am. J. Physiol.* 234:H312–314.

29. Weld, F. M., J. Coromilas, J. N. Rottman, and J. T. Bigger, Jr. 1982. Mechanisms of quinidine-induced depression of maximum upstroke velocity in ovine cardiac Purkinje fibers. *Circ. Res.* 50:369–376.

30. Courtney, K. R. 1983. Quantifying antiarrhythmic drug blocking during action potentials in guinea-pig papillary muscle. *J. Mol. Cell. Cardiol.* 15:749–757.

31. Hondeghem, L. M., and T. Matsubara. 1984. Quinidine and lidocaine: activation and inactivation block. *Proc. West. Pharmacol. Soc.* 27:19–21.

32. Colatsky, T. J. 1985. Actions of local anesthetics and antiarrhythmics on membrane channels in the heart. *In* Effects of Anesthesia. B. G. Covino, H. A. Fozzard, K. Rehder, and G. Strichartz, editors. American Physiological Society, Bethesda, MD.

33. Starmer, C. F., D. L. Packer, and A. O. Grant. 1987. Ligand binding to transiently accessible sites: mechanisms for varying apparent binding rates. *J. Theor. Biol.* 124:335–341.

34. Starmer, C. F., A. O. Grant, and H. C. Strauss. 1984. Mechanisms of use-dependent block of sodium channels in excitable membranes by local anesthetics. *Biophys. J.* 46:15–27.

35. Starmer, C. F., and A. O. Grant. 1985. Phasic ion channel blockade: a kinetic model and parameter estimation procedure. *Mol. Pharmacol.* 38:348–356.

36. Starmer, C. F. 1986. Theoretical characterization of ion channel blockade: ligand binding to periodically accessible receptors. *J. Theor. Biol.* 119:235–249.

37. Starmer, C. F., and R. B. Kerr. 1985. Simulation of use-dependent uptake of ion channel blocking agents by excitable membrances. *IEEE (Inst. Electr. Electron. Eng.) Trans. Biomed. Eng.* 32:770–774.

38. Starmer, C. F., and M. D. Hollett. 1985. Mechanisms of apparent affinity variation of guarded receptors. *J. Theor. Biol.* 115:337–349.

39. Starmer, C. F., and K. R. Courtney. 1986. Simulation of use-

dependent uptake of ion channel blockade at guarded binding sites: application to tertiary drugs. *Am. J. Physiol.* 251:H848–H856.

40. Hondeghem, L. M., and B. G. Katzung. 1977. Time- and voltage-dependent interactions of antiarrhythmic drugs with cardiac sodium channels. *Biochim. Biophys. Acta.* 472:373–398.

41. Courtney, K. R., J. J. Kendig, and E. N. Cohen. 1978. The rates of interaction of local anesthetics with sodium channels in nerve. *J. Pharmacol. Exp. Ther.* 207:595–604.

42. Khodorov, B., L. Shishkova, E. Peganov, and S. Revenko. 1976. Inhibition of sodium currents in frog Ranvier node treated with local anesthetics. Role of slow inactivation. *Biochim. Biophys. Acta.* 433:409–435.

43. Hille, B. 1977. Local anesthetics: hydrophilic and hydrophobic pathways for the drug-receptor reaction. *J. Gen. Physiol.* 69:497–515.

44. Wallace, A. G., R. E. Cline, W. C. Sealy, W. G. Young, Jr., and W. G. Troyer. 1966. Electrophysiologic effects of quinidine: studies using chronically implanted electrodes in awake dogs with and without cardiac denervation. *Circ. Res.* 19:960–969.

45. Hondeghem, L. M. 1978. Validity of $\dot{V}_{max}$ as a measure of the sodium current in cardiac and nervous tissue. *Biophys. J.* 23:147–152.

46. Coromilas, J., F. M. Weld, and J. T. Bigger, Jr. 1981. Validity of maximum upstroke velocity as a measure of peak sodium conductance in cardiac Purkinje fiber. *Circulation.* 64:(Suppl. IV):115. (Abstr.)

47. Cohen, I. S., and G. R. Strichartz. 1977. On the voltage-dependent action of tetrodotoxin. *Biophys. J.* 17:275–279.

48. Cohen, C. J., P. Bean, and R. W. Tsien. 1984. Maximal upstroke velocity as an index of available sodium conductance. *Circ. Res.* 54:636–651.

49. Fozzard, H., D. A. Hanck, and M. F. Sheets. 1986. Non-linear relationship of maximal upstroke velocity to the sodium current in single canine Purkinje cells. *J. Physiol. (Lond.).* 382:103P.

50. Sheets, M. F., D. A. Hanck, and H. A. Fozzard. 1987. Quinidine alters the relationship of $\dot{V}_{max}$ to N_a current in single cardiac Purkinje cells. *Circulation.* 76:149. (Abstr.)

51. Grant, A. O., J. L. Trantham, K. K. Brown, and H. C. Strauss. 1982. pH-dependent effects of quinidine on the kinetics of dV/dt max in guinea pig ventricular myocardium. *Circ. Res.* 50:210–217.

52. Yeh, J. Z., and J. Tanguy. 1985. The Na channel activation gate modulates slow recovery from use-dependent block by local anesthetics in squid giant axons. *Biophys. J.* 47:685–694.

53. Wang, G. K., M. S. Brodwick, D. C. Eaton, and G. R. Strichartz. 1987. Inhibitation of sodium currents by local anesthetics in chloramine T-treated squid axons. *J. Gen. Physiol.* 89:645–667.

54. Chen, C. M., and L. S. Gettes. 1976. Combined effects of rate, membrane potential, and drugs on maximum rate of rise ($\dot{V}_{max}$) of action potential upstroke of guinea pig papillary muscle. *Circ. Res.* 38:464–469.

55. Chen, C. M., L. S. Gettes, and B. G. Katzung. 1975. Effect of lidocaine and quinidine on steady-state characteristics and recovery kinetics of (dV/dt_{max}) in guinea pig ventricular myocardium. *Circ. Res.* 37:20–29.

56. Bean, B. P., C. J. Cohen, and R. W. Tsien. 1983. Lidocaine block of cardiac sodium channels. *J. Gen. Physiol.* 81:613–642.

57. Browning, D. J., and H. C. Strauss. 1981. Effects of stimulation frequency on potassium activity and cell volume in cardiac tissue. *Am. J. Physiol.* 240:C39–C55.

58. Kunze, D. L. 1977. Rate-dependent changes in extracellular potassium in the rabbit atrium. *Circ. Res.* 41:122–127.

59. Kline, R., and M. Morad. 1976. Potassium efflux and accumulation in heart muscle: evidence from K+ electrode experiments. *Biophys. J.* 16:367–372.

60. Vassalle, M. 1970. Electrogenic suppression of automaticity in sheep and dog Purkinje fibers. *Circ. Res.* 27:361–377.

61. Courtney, K. R. 1980. Interval-dependent effects of small antiarrhythmic drugs on excitability of guinea-pig myocardium. *J. Mol. Cell. Cardiol.* 12:1273–1286.

62. Weld, F. M., and J. T. Bigger, Jr. 1975. Effect of lidocaine on the early inward transient current in sheep cardiac Purkinje fibers. *Circ. Res.* 37:630–639.

63. Packer, D. L., K. C. Courtney, and C. F. Starmer. 1987. M gate guarding and absence of trapping supported by directly determined rate constants from Na+ channel blockade by the lidocaine analogue W36017. *Circulation.* 76:IV-148. (Abstr.)

64. Kojima, M., and T. Ban. 1988. Nicorandil shortens action potential duration and antagonizes the reduction of $\dot{V}_{max}$ by lidocaine but not disopylamide in guinea pig papillary muscles. *Naunyn-Schmiedebergs Arch. Pharmakol.* 337:203–212.

65. Arnsdorf, M. F., and G. J. Sawicki. 1987. Effects of quinidine sulfate on the balance among active and passive cellular properties that comprise the electrophysiologic matrix and determine excitability in sheep Purkinje fibers. *Circ. Res.* 61:244–255.

66. Bennett, P. B., and L. M. Hondeghem. 1988. Inhibition of sodium conductance by quinidine: Single channel blocking mechanisms. *Circulation.* 78:II-410. (Abstr.)

67. Grant, A. O., and C. F. Starmer. 1987. Mechanism of closure of sodium channels in rabbit ventricular myocytes: Single channel analysis. *Circ. Res.* 60:897–913.